

# Harmonic motion imaging for focused ultrasound (HMIFU): a fully integrated technique for sonication and monitoring of thermal ablation in tissues

C Maleke<sup>1</sup> and E E Konofagou<sup>1,2</sup>

<sup>1</sup> Department of Biomedical Engineering, Columbia University, NY, USA

<sup>2</sup> Department of Radiology, Columbia University, NY, USA

E-mail: [cm2243@columbia.edu](mailto:cm2243@columbia.edu) and [ek2191@columbia.edu](mailto:ek2191@columbia.edu)

Received 22 October 2007, in final form 10 February 2008

Published 6 March 2008

Online at [stacks.iop.org/PMB/53/1773](http://stacks.iop.org/PMB/53/1773)

## Abstract

FUS (focused ultrasound), or HIFU (high-intensity-focused ultrasound) therapy, a minimally or non-invasive procedure that uses ultrasound to generate thermal necrosis, has been proven successful in several clinical applications. This paper discusses a method for monitoring thermal treatment at different sonication durations (10 s, 20 s and 30 s) using the amplitude-modulated (AM) harmonic motion imaging for focused ultrasound (HMIFU) technique in bovine liver samples *in vitro*. The feasibility of HMI for characterizing mechanical tissue properties has previously been demonstrated. Here, a confocal transducer, combining a 4.68 MHz therapy (FUS) and a 7.5 MHz diagnostic (pulse-echo) transducer, was used. The therapy transducer was driven by a low-frequency AM continuous signal at 25 Hz, producing a stable harmonic radiation force oscillating at the modulation frequency. A pulser/receiver was used to drive the pulse-echo transducer at a pulse repetition frequency (PRF) of 5.4 kHz. Radio-frequency (RF) signals were acquired using a standard pulse-echo technique. The temperature near the ablation region was simultaneously monitored. Both RF signals and temperature measurements were obtained before, during and after sonication. The resulting axial tissue displacement was estimated using one-dimensional cross correlation. When temperature at the focal zone was above 48 °C during heating, the coagulation necrosis occurred and tissue damage was irreversible. The HMI displacement profiles in relation to the temperature and sonication durations were analyzed. At the beginning of heating, the temperature at the focus increased sharply, while the tissue stiffness decreased resulting in higher HMI displacements. This was confirmed by an increase of  $0.8 \mu\text{m } ^\circ\text{C}^{-1}$  ( $r = 0.93$ ,  $p < .005$ ). After sustained heating, the tissue became irreversibly stiffer, followed by an associated decrease in the HMI displacement ( $-0.79 \mu\text{m } ^\circ\text{C}^{-1}$ ,  $r = -0.92$ ,  $p < 0.001$ ). Repeated experiments showed a reproducible pattern of the HMI displacement changes with a temperature at a slope equal to

$0.8 \pm 0.11$  and  $-0.79 \pm 0.14 \mu\text{m } ^\circ\text{C}^{-1}$ , prior to and after lesion formation in seven bovine liver samples, respectively. This technique was thus capable of following the protein-denatured lesion formation based on the variation of the HMI displacements. This method could, therefore, be applied for real-time monitoring of temperature-related stiffness changes of tissues during FUS, HIFU or other thermal therapies.

(Some figures in this article are in colour only in the electronic version)

## 1. Introduction

Over the past 60 years, researchers have investigated the potential of utilizing focused ultrasound (FUS) (or, high intensity focused ultrasound (HIFU)) as a minimally, or non-invasive, cancer treatment modality. FUS generates an acoustic wave that propagates through soft tissue and deposits a high level of acoustic energy mainly at the localized focus of the transducer. High levels of acoustic energy at the localized focus can cause temperature elevation that is sufficient to initiate coagulative necrosis in tissues (thermal lesions), while the surrounding tissues remain relatively unheated. The ability of FUS to cause irreversible damage in tissues has received attention from researchers as a potential technique for non-invasive cancer treatment. Lynn *et al* (1943) and Lynn and Putnam (1944) introduced one of the first applications of FUS for local modification of brain function in live animals, e.g., cats and dogs. Fry *et al* (1954), (1955) and Lele (1967) continued the development of FUS therapy and produced lesions deep in the brains of cats and monkeys. The application of FUS was later introduced for cancer treatment in 1956 (Burov and Andreevskaya 1956, Taylor and Connolly 1969). FUS surgery has continued to be an area of intense research, well into the present day (Linke *et al* 1973, Fry and Johnson 1978, Bamber and Hill 1979, Corry *et al* 1984, Goss and Fry 1984, Frizzell 1988, Kennedy *et al* 2003).

In ultrasound therapy, an FUS transducer induces a high level of acoustic intensity at a localized focus for a short duration. The rise in temperature corresponds to the transformation of acoustic energy into thermal energy as the ultrasound waves are absorbed by the tissue. Thus, the extent of the tissue damage depends on the exposure time and temperature rise (Ter Haar 1995, Vykhodtseva *et al* 1995, Sanghvi *et al* 1996). FUS was shown capable of inducing a complete tumor necrosis for the treatment of human prostate cancer *in vivo* (Gelet *et al* 1996, 1999, Madersbacher *et al* 1995, Wu 2006). Two major limitations of FUS surgery include the difficulty of monitoring the changes in temperature and tissue mechanical properties as well as the lack of ability to optimally control precise thermal exposure upon lesion formation.

Conventional B-mode ultrasound imaging has been widely used to visualize the progress of thermal therapy (Lele 1966, Ter Haar *et al* 1989, Yang *et al* 1993). However, this imaging technique is not optimal to identify coagulative tissue because the tissue echogenicity does not change significantly during thermal therapy (Hill and Ter Haar 1995, Ter Haar 1995, Hynynen 1997). The coagulative tissues can only be detected when cavitation, or boiling, occurs due to the high bubble concentrations that cause hyperechoic appearance in the treated area (Vaezy *et al* 1997, Chavrier *et al* 2000, Kennedy 2005). However, bubble occurrence is usually unpredictable, and therefore unreliable for FUS treatment monitoring. Several noninvasive temperature monitoring methods for FUS therapy have been proposed for estimating thermal dose, such as ultrasound and magnetic resonance imaging (MRI) and MRI thermometry.

Ultrasound elastography was shown capable of assessing the extent of thermal ablation in rabbit paraspinal skeletal muscle *in vitro* (Stafford *et al* 1998, Kallel *et al* 1999), bovine liver *in vitro* (Righetti *et al* 1999) and human prostate *in vivo* (Souchon *et al* 2003) due to its sensitivity to stiffness changes. Souchon *et al* 2003 showed a 40%–50% decrease in average strain in the treated region of the human prostate *in vivo* after FUS application. However, the required external tissue compression may complicate positioning and reference during treatment planning and guidance.

Non-invasive temperature-induced echo-shift imaging is based on the fact that the speed of sound in non-fatty tissues increases with temperature. The FUS transducer generates localized heating at the focus producing changes in tissue characteristics. These changes are related to the speed of sound and tissue thermal expansion that cause echo shifts in the backscattered ultrasonic signal. These findings have been validated theoretically and experimentally in non-invasive thermal therapy (Seip and Ebbini 1995, Pernot *et al* 2004, Arthur *et al* 2005).

MRI has been used for noninvasive guidance and monitoring of thermal therapies, because it can provide quantitative spatial maps of the induced temperature rise at high spatial resolution (Cline *et al* 1995, Gellermann *et al* 2005, Anand *et al* 2007). This technique is known as MR-guided FUS surgery (Cline *et al* 1995, Huber *et al* 2001, Hynynen *et al* 2001, Gianfelice *et al* 2003, Furusawa *et al* 2006). The FUS transducer is positioned over the cancerous tissue, while magnetic resonance imaging (MRI) is used to detect the tumor and monitor the ablation process. In the magnetic resonance elastography technique (MRE), tissue mechanical properties (e.g., shear modulus) are mapped based on the observed phase shift of the MR signal, in response to an external mechanical vibration (Lewa 1991, Muthupillai *et al* 1995, Sinkus *et al* 2000). Wu *et al* (2001) showed that the MRE was able to quantitatively estimate the differences in mechanical properties (shear modulus) between the ablated and the normal tissues. Furthermore, the MRE results indicated that the ablated tissues were stiffer than the normal tissues. Despite these initial successes of FUS-surgery monitoring using the MR-based imaging techniques, the lack of low-cost and reliable monitoring methods at high temporal resolution may result in the confinement of this promising treatment to large research centers worldwide (Kennedy 2005). More precisely, the FUS technique is in itself a low-cost treatment technique that covertly requires a high-cost monitoring device, i.e., an MRI system.

The vibroacoustography method uses two confocal ultrasound beams to generate a localized oscillatory radiation force in tissue. The resulting tissue displacement produces a localized acoustic source that emits an acoustical signal recorded by a hydrophone (Fatemi and Greenleaf 1998). Recent studies have shown that an oscillatory acoustic radiation force can be generated in biological soft tissues at variable depths within the tissue (Sarvazyan *et al* 1998, Fatemi and Greenleaf 2000, Konofagou *et al* 2001, Konofagou and Hynynen 2002, 2003, Michishita *et al* 2003, Bercoff *et al* 2004a, Bercoff *et al* 2004b). Konofagou *et al* (2002), (2003) applied the vibroacoustography technique for both temperature monitoring of thermal therapy and thermal lesion formation. This technique relied on the principles of two focused beams at slightly different frequencies that generated a radiation force at the overlapped focus. However, the effect of temperature-induced acoustic changes (e.g., speed of sound change) could not be separated from the effect of mechanical changes.

The use of radiation-force-based monitoring during tissue ablation has also been investigated by Lizzi *et al* (2003) and Fahey *et al* (2004). They developed a method to monitor the formation of lesions during FUS therapy using the acoustic radiation force impulse (ARFI) technique in *in vitro* and *ex vivo* tissues. ARFI induces a brief localized radiation force and images the tissue response immediately after force application, using a modified linear array transducer (Nightingale *et al* 2001). The tissue displacements are estimated using a speckle-tracking technique. After FUS treatment, the results showed that the displacement was much

smaller in the coagulated tissue than in the normal tissue (Lizzi *et al* 2003). A limitation of the aforementioned techniques for ultrasound therapy monitoring is that, currently, tissue displacement cannot be monitored during force application due to the use of pushing and tracking beams at different times.

Harmonic motion imaging (HMI) is a radiation-force technique that induces oscillatory displacements at the focal zone of the FUS transducer for the detection of localized stiffness changes (Konofagou and Hynynen 2003). We recently introduced an amplitude-modulated (AM) version of the HMI method that produced the harmonic radiation force using a single-element FUS (therapy) transducer (Maleke *et al* 2006) instead of the previous two-transducer configuration (Konofagou and Hynynen 2003). The AM beam offered the advantages of a simpler transducer design and a sustained application of the radiation force at a stable focus within the tissue region (Maleke *et al* 2006). In Maleke *et al* (2006), we described the feasibility of the amplitude-modulated (AM) HMI technique for thermal ablation monitoring, with alternating continuous (for ablation) and AM (for HMI) signals during heating. Here, we developed a new method that uses the amplitude modulation throughout, i.e., for *simultaneous* HMI and ablation during the entire treatment. Since we applied an oscillatory motion and measured peak-to-peak displacements, the motion induced in the tissue is independent of the duration of the applied force, assuming tissue elasticity stays constant (no softening/hardening) during force application. The purpose of this study was to investigate the temperature dependence of the HMI technique during sonication. This method offers the ability to monitor the ablation process non-invasively through filtering of the therapy beam. Most importantly, a major advantage of this technique is the real-time feedback of the resulting variation in tissue mechanical properties during thermal treatment.

When used for monitoring of thermal ablation using focused ultrasound (FUS), the integrated system is hereby named HMIFU for harmonic motion imaging for focused ultrasound. We therefore applied the HMIFU system with two separate applications in mind. The first application was to assess tissue stiffness changes before and after thermal ablation. The therapy transducer in this case was driven by AM pulses at low acoustic powers, but sufficient to induce adequate motion with an associated negligible temperature rise. In its second application, a higher acoustic power was applied for generating *and* simultaneously monitoring thermal ablation. The resulting synchronous monitoring system has the ability to follow and identify the areas of necrosis. The ultimate future goal is to generate, and simultaneously monitor, lesion formation over the region without interrupting the treatment of a targeted tumor in organs such as the liver and the pancreas, with a precise and optimal treatment time (i.e. based on the thermal dose) as well as a controlled lesion size (figure 1).

## 2. Theory

In HMI, an AM wave is generated through addition and multiplication of two continuous signals with two different frequencies, e.g., a carrier frequency at 4.68 MHz ( $f_c$ ) and a modulation frequency at 25 Hz ( $f_m$ ). The average power density or intensity for an AM wave is  $p = p_+ \cdot \cos(2\pi f_c t - kz) \cdot \cos(2\pi f_m t - kz)$ , where  $p_+$  is an amplitude constant, can be calculated by (Christensen 1988)

$$\bar{I} = \frac{1}{\lambda} \int_0^\lambda \frac{p^2}{Z} dz, \quad (1)$$

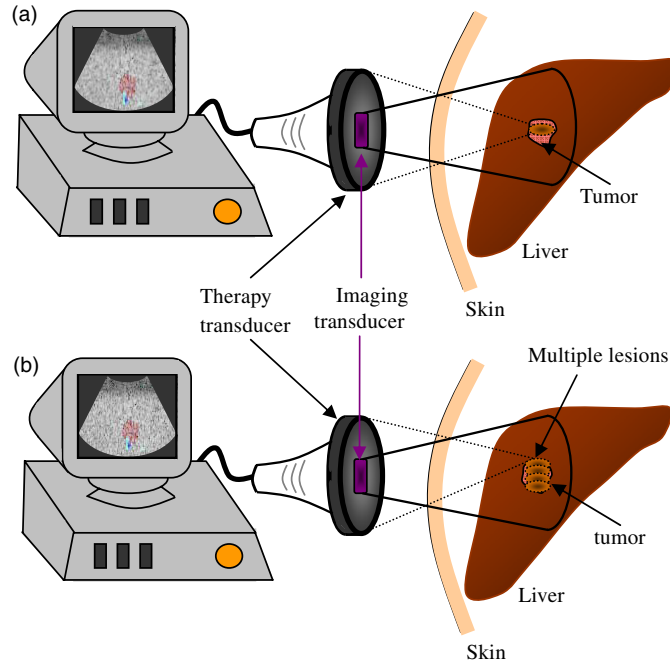


**Figure 1.** (a) Detection of the area to be ablated (e.g. tumor) using the HMIFU technique, (b) FUS ablation and simultaneous monitoring in order to map the response of the tumor overlapped on the B-mode in 2D as will be displayed on the screen together with the M-mode HMI image (not shown here).

where  $Z$  is the acoustic impedance,  $z$  is the depth,  $\lambda$  is the wavelength and  $k$  is the wavenumber. The acoustic intensity ( $\bar{I}$ ) calculation is simply an integration of the instantaneous power density over one wavelength, and thus  $\bar{I}$  is given by (Christensen 1988)

$$\bar{I} = \frac{k}{2\pi} \int_0^{2\pi/k} \frac{p_+^2}{Z} \cdot \cos^2(2\pi f_c t - kz) \cdot \cos^2(2\pi f_m t - kz) dz = \frac{kp_+^2}{2\pi Z} \cdot \frac{2\pi}{4k} = \frac{p_+^2}{4Z}. \quad (2)$$

The acoustic intensity ( $\bar{I}$ ) for an AM wave is half of that of a non-modulated acoustic wave. Thus, a higher energy or a longer heating time is needed in order to ablate tissue and produce a similar lesion size formed by a conventional pulsed or continuous sinusoidal wave.

The area of thermal coagulation observed during heating corresponds to a mathematical model that provides apparent distinction on temperature effects in tissues. The thermal dose is used as a measure for predicting the extent of tissue damage caused by heating exposure. It is derived from *in vitro* cell survival experiments during hyperthermia, when the cells were exposed to temperatures from 43 °C to 50 °C (Sapareto and Dewey 1984). Damianou *et al* also reported that a lethal dose was found at and beyond 43 °C (1997). The effect of heating and the equivalent heating time at 43 °C in hyperthermia can be described by the following empirical model (Sapareto and Dewey 1984), i.e.,

$$t_{43} = \sum_{t=0}^{t=\text{final}} k^{(43-T_t)} \Delta t, \quad (3)$$

where  $t_{43}$  is the equivalent time at 43 °C,  $T_t$  is the average temperature during the short time of heating time ( $\Delta t$ ) and  $k = 0.5$  above 43 °C for many tissues and  $k = 0.25$  below 42 °C. This

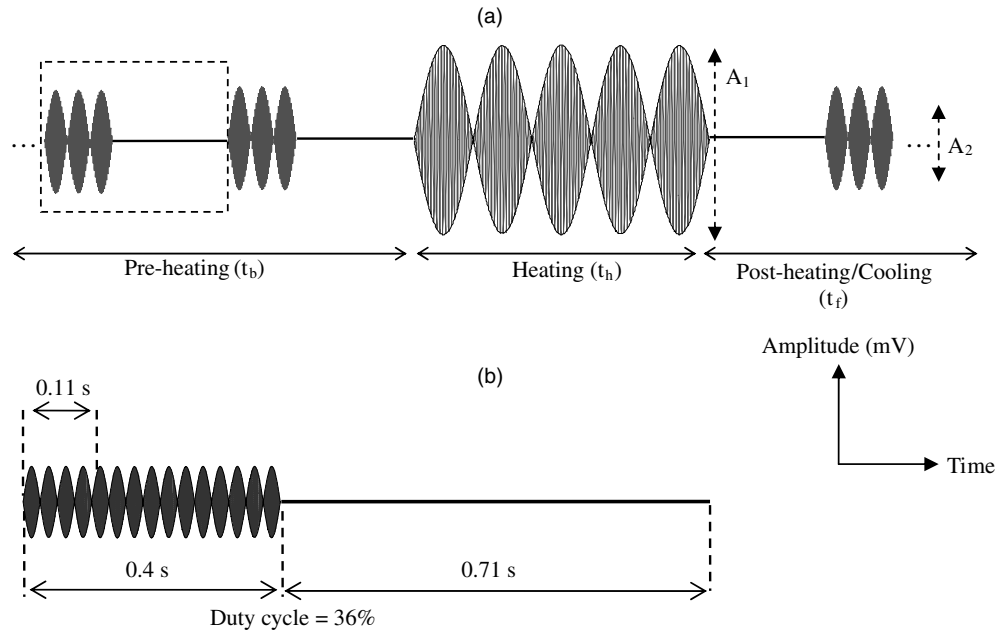


**Figure 2.** (a) The HMIFU technique consists of two types of AM waves: (1) a continuous AM for heating ( $t_h$ ) and (2) a pulsed AM for before ( $t_b$ ) and after ( $t_f$ ) heating. The acoustic intensities for  $A_1$  and  $A_2$  were 600 mV<sub>pp</sub> and 300 mV<sub>pp</sub> respectively. (b) Detailed representation of the dashed rectangle in (a).

model was used in section 3.2 to verify the onset of coagulative necrosis during ablation. The threshold calculation ( $t_{43}$ ) and the measured temperature values along with the estimated HMI displacements were compared at different sonication durations.

### 3. Methods

#### 3.1. Tissue sample preparation

Experiments were performed in seven ( $n = 7$ ) *in vitro* bovine liver specimens with three ( $m = 3$ ) different locations in each liver, i.e., 21 locations in total. Sample tissues were purchased from a grocery store and degassed in phosphate buffered saline (PBS) solution for 30 min prior to each experiment. The average size of all seven bovine liver specimens used was  $120 \times 50 \times 12 \text{ mm}^3$  (LxWxD). Each specimen was then placed into a glass beaker and submerged in PBS. A hot plate/stirrer (Corning PC-420, Corning, NY, USA) was positioned underneath the glass beaker to maintain a uniform temperature of  $37^\circ\text{C}$  throughout the entire tissue specimen to simulate human body temperature.

#### 3.2. Experimental setup and data acquisition

For this study, a continuous AM wave was used during heating and a pulsed AM signal was applied off-heating, i.e., before and after heating (figure 2). A pulsed AM was applied to avoid any significant temperature rise during HMI monitoring. The acoustic intensities (equation (2)) at the focus were  $1086 \text{ W cm}^{-2}$  during heating and  $231 \text{ W cm}^{-2}$  before and after heating in

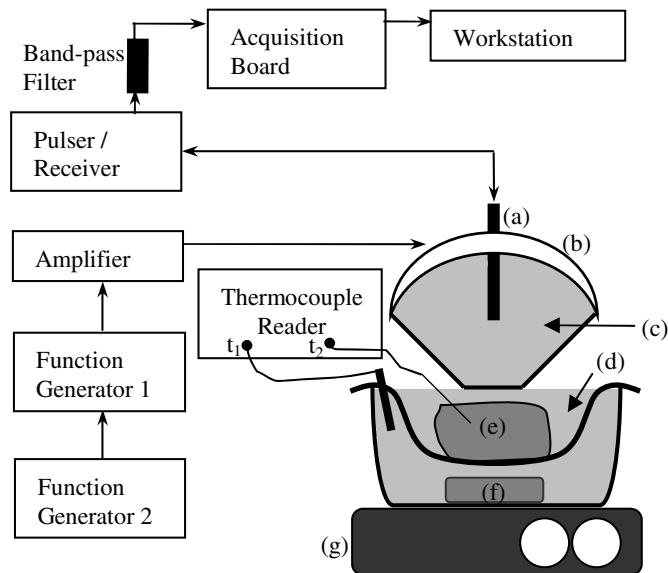


**Figure 3.** Block diagram of the experimental setup. (a) Pulse-echo transducer, (b) therapy transducer and (c) degassed water. The specimen (or, phantom gels) (e) rests on a membrane and is submerged in PBS (d). In order to reduce possible reflections, i.e., specular reflection, an absorber (f) is placed on the bottom of the glass beaker. A hot plate/stirrer (g) maintains the surrounding temperature at 37 °C. Two thermocouples,  $t_1$  and  $t_2$ , are used to measure the external and specimen temperatures, respectively.

order to avoid significant temperature rise during the latter. These parameters were selected based on prior studies (Maleke *et al* 2006).

A 4.68 MHz therapy transducer (Riverside Research Institute, New York, NY, USA) was used to generate the acoustic radiation force using a low-frequency, amplitude-modulated RF signal. The focal region has an ellipsoidal shape with the long axis parallel to the ultrasound beam. The  $-6$  dB dimensions are 4.0 mm in the axial direction and 0.5 mm in the lateral direction. The low-frequency AM waves were expected to provide sufficiently deep penetration of the elastic wave through tissues (Sinkus *et al* 2006). RF signals were acquired continuously before, during and after sonication at approximately 0.71 s intervals. By examining the displacement amplitudes before and after heating, the relative stiffness change can be followed. In this experiment, the sonication duration was within the range of 5 s to 30 s. The experimental setup is shown in figure 3. A frequency generator (Agilent (HP) 33120A, Palo Alto, CA, USA) was used to produce RF signals at 4.68 MHz. The amplitude of RF signals was then modulated using a second frequency generator (Agilent (HP) 33220A, Palo Alto, CA, USA) that generated a low-frequency modulation at 25 Hz, for a pulse of 10 cycles with a duty cycle of 36% (figure 2(b)).

The HMI technique produces an oscillatory motion at the modulation frequency ( $f_m$ ). The modulation index ( $m$ ) is defined as the ratio of the maximum to the minimum voltage of the modulated signal. The conventional amplitude modulation has a modulation index ( $m$ ) equal to 1 (i.e. 100% modulation), which indicates that the magnitude of the modulating signal (low frequency or  $f_m$ ) is equal in magnitude to that of the carrier signal (high frequency or  $f_c$ ). If this conventional amplitude modulation is applied to generate an oscillating radiation force, the resulting acoustic pressure at the focus would consist of three oscillatory frequencies,

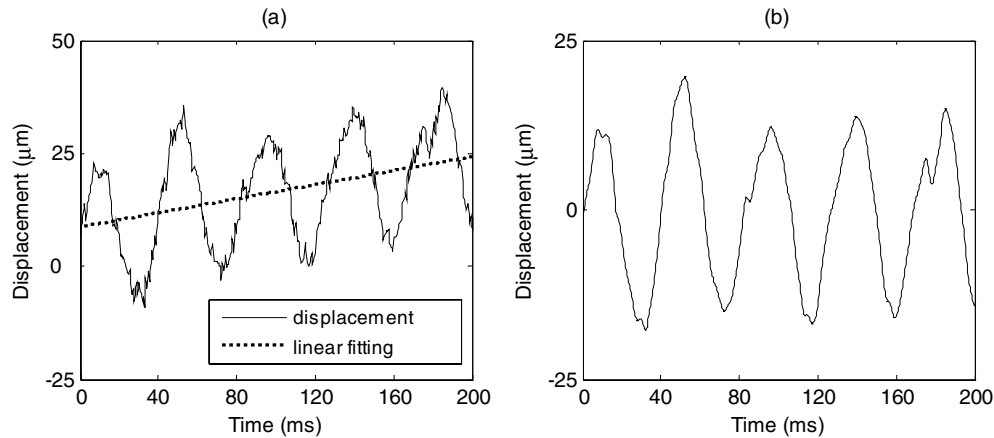


**Figure 4.** (a) Displacement with speed of sound effect during heating and (dotted line) is a linear fitting. (b) Displacement after removal of the speed of sound effect and the application of low-pass filtering.

i.e.,  $f_c, f_c \pm f_m$ , where  $f_c$  and  $f_m$  represent the carrier frequency and modulation frequency, respectively. The carrier signal was thus over-modulated ( $m \geq 50$ ) to induce oscillation of the resulting acoustic pressure and, subsequent displacement, at the only desired frequency, i.e.,  $f_m$  (Maleke *et al* 2006).

The fact that speed of sound changes as a function of temperature has been reported to induce an artifactual shift in the backscatter ultrasonic signal or, a temperature-induced displacement (Seip *et al* 1996). The estimated displacement at the focal region is proportional to its temperature rise. As shown in figure 4, our technique could follow the changes in the speed of sound when an AM wave was applied for heating, which was indicated simply by a linear trend (slope =  $0.63 \text{ mm s}^{-1}$ ) of the oscillatory displacement (dotted line in figure 4(a)). This linear trend was successfully separated from the oscillatory HMI displacement and the high-frequency spectrum was also filtered out. The harmonic displacement at the modulating frequency was thus used to estimate the resulting displacements (figure 4(b)). The displacement and speed of sound are linearly proportional (Seip *et al* 1996) and the speed of sound is known to vary linearly with temperature in the liver tissue, hence the linear trend. One of the advantages of the HMI method is thus the successful removal of the harmonic (real) displacement from a linear speed-of-sound-dependent (artifact) displacement for decoupling and estimation of both speed of sound and stiffness effects.

A pulse-echo transducer (Panametrics, Waltham, MA, USA) with a center frequency of 7.5 MHz and a diameter of 12 mm was placed through the void center of the FUS transducer, with the beams of the two transducers being confocal. A pulser/receiver (Panametrics 5051PR, Waltham, MA, USA) was used to drive the pulse-echo transducer at a PRF of 5.4 kHz. The RF signals were acquired using a standard pulse-echo technique. An analog bandpass filter (Reactel, Inc., Gaithersburg, Maryland, USA) with cutoff frequencies of  $f_{c1} = 5.84 \text{ MHz}$  and  $f_{c2} = 8.66 \text{ MHz}$  was used to filter out the high-frequency focused beam and its harmonics (Maleke *et al* 2006).

A silicone rubber/absorber (McMaster-Carr, Dayton, NJ, USA) was placed beneath the specimen to further reduce the specular reflection from the bottom of the glass container. The filtered RF signals were captured at 80 MHz at a 14 bit digitization rate (CS14200, Gage Applied Technologies, Lachine, Canada).

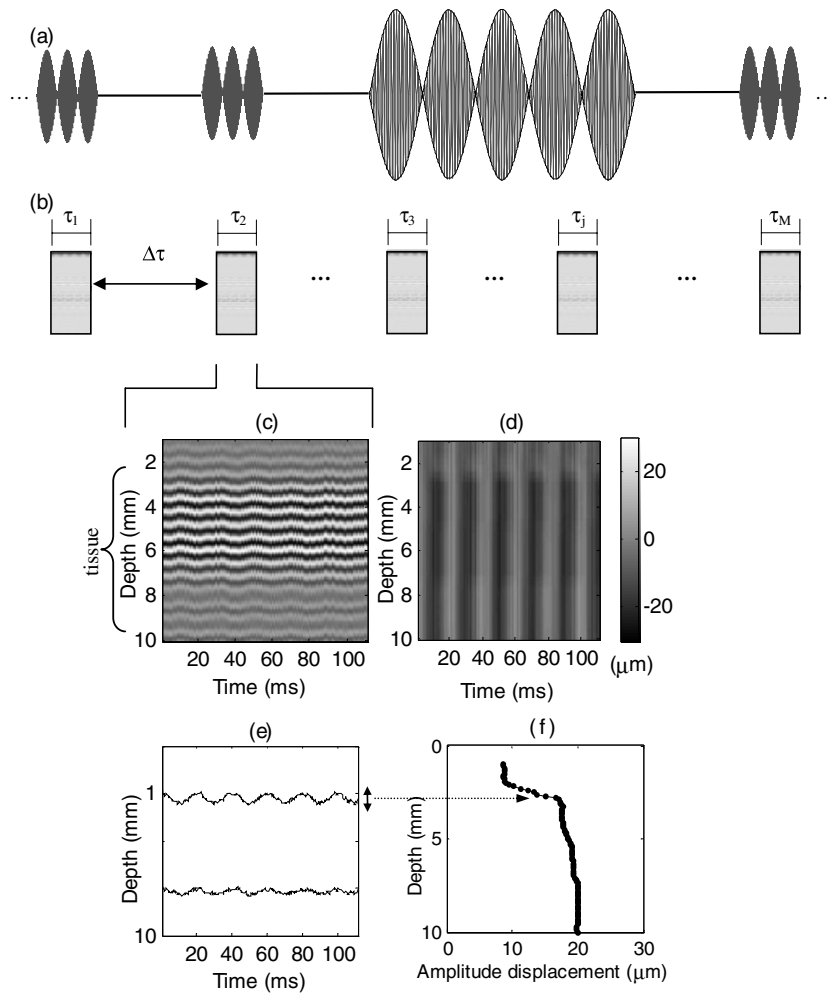


**Figure 5.** (a) Schematic of the acquisition process for the HMIFU experiment. (b) M-mode frames are acquired at 1.11 s intervals ( $\Delta\tau$ ), i.e., the frame rate is equal to 1.8 frame  $s^{-1}$ . (c) one M-mode RF frame ( $\tau_n$ , for  $n = 1, 2, \dots, j, \dots, M$ ;  $M$  = the entire treatment time), has a period of 111 ms, such that each frame includes at least two periods of AM oscillations. (d) M-mode HMI displacement image at the focal region. (e) peak-to-peak displacement was estimated at all depths and plotted with respect to depth, (f).

### 3.3. HMI imaging

Sequences of M-mode frames were acquired before, during and after heating (figure 5). Each M-mode frame (figure 5(c)) contained 600 RF lines and had a duration of  $\tau = N/\text{PRF} = 111$  ms, where  $N$  was the number of RF lines ( $N = 600$ ) and PRF was 5.4 kHz; thus, each frame spanned over two periods of AM oscillations. The time interval ( $\Delta\tau$ ) between two consecutive M-mode frames was approximately 1.11 s, i.e., the frame rate was equal to 1.8 frame  $s^{-1}$ . One-dimensional, cross-correlation on consecutive RF signals was applied to the acquired M-mode frames with a kernel size equal to 0.47 mm, 90% overlap (Ophir *et al* 1997) to estimate cumulative axial displacements (figure 5(d)) resulting from the radiation force, with the first oscillation serving as the reference. The peak-to-peak displacement was

estimated at all depths (figure 5(e)) and plotted with respect to depth, as seen in figure 5(f). These steps were applied for every RF frame acquired at different times and the resulting depth-dependent peak-to-peak displacements were plotted against time. The time needed to generate the entire M-mode frames was approximately 30 s. The variation in HMI displacement can be clearly visualized in the M-mode maps, which were used in detecting the tissue coagulation.

The highest spectral peak was centered on a low-frequency excitation ( $f_m$ ). The  $f_m$  in this experiment was 25 Hz; thus, the highest peak of the spectrum was located at 25 Hz. In order to estimate the displacement amplitude (HMI displacement), the peak of the displacement spectra was divided by the number of samples and then normalized by the input signal amplitude ( $A_1$  or  $A_2$ ; figure 2).

### 3.4. Temperature measurements

A type T thermocouple (MT-29, Physitemp Instruments, Inc., Clifton, New Jersey, USA) with a diameter of 0.33 mm was inserted into the *in vitro* tissue to independently monitor temperature change before, during and after heating. First, the therapy transducer was attached to a computer-controlled positioner (Velmex Inc., Bloomfield, NY, USA) and driven at a low acoustic power level. Once the thermocouple was inserted into the tissue, the positioner was used to locate the tip of the thermocouple, which was indicated by a rapid temperature increase and high amplitude echo from the confocal pulse-echo transducer. Thus, we could roughly estimate that the therapy beam was approximately aligned with the tip of the thermocouple. A digital thermocouple reader (HH506A, Omega Engineering, Stamford, CT, USA) was used to record the temperature at 1 s intervals.

## 4. Results

To investigate the temperature effects of different AM inputs during monitoring, we applied pulsed (figure 6(b)) and continuous (figure 6(a)) AM waves to a gelatin phantom (Hall *et al* 1997, Maleke *et al* 2006) and recorded the temperature increase at various thermocouple positions near the focus for a 40 s exposure. Both waveforms were generated by the same low acoustic intensity of  $231 \text{ W cm}^{-2}$ . The homogeneous structure of the gelatin phantom allowed us to independently measure temperature for the two different input waveforms. This experiment was conducted using the same setup as in figure 2, with a tissue-mimicking phantom having a stiffness of 40 kPa (Hall *et al* 1997) placed inside the container (figure 2(e)). The application of pulsed AM shows a relatively constant temperature ( $\Delta T_{\max} \sim 1.2 \text{ }^\circ\text{C}$ ) compared to that induced by the continuous AM wave.

Figure 7 depicts the HMI displacement against time with blue, red and green lines indicating baseline, heating and cooling periods, respectively. The baseline period duration was 5 s in all cases, sonication period varied from 10 s to 30 s (a to c) and the cooling period was 10 s in all cases. To better understand the stiffness changes in the AM thermal-ablated *in vitro* liver tissue, we applied 5 s pulsed AM wave for pre- and 10 s post-heating phases. The liver tissue was heated using an AM therapeutic beam that induced both an oscillatory motion and heating of the tissue. This oscillatory displacement increases at the beginning during heating, indicating tissue softening. If the heating is sustained, the displacement decreases, which denotes that the tissue becomes stiffer, i.e., a lesion has been formed. We believe that this pattern of tissue displacement change reflects the heat-induced structural changes in tissue. This is verified during cooling, when the displacements are slightly lower compared to the baseline (pre-heating) period. In this preliminary study, experimental results show that

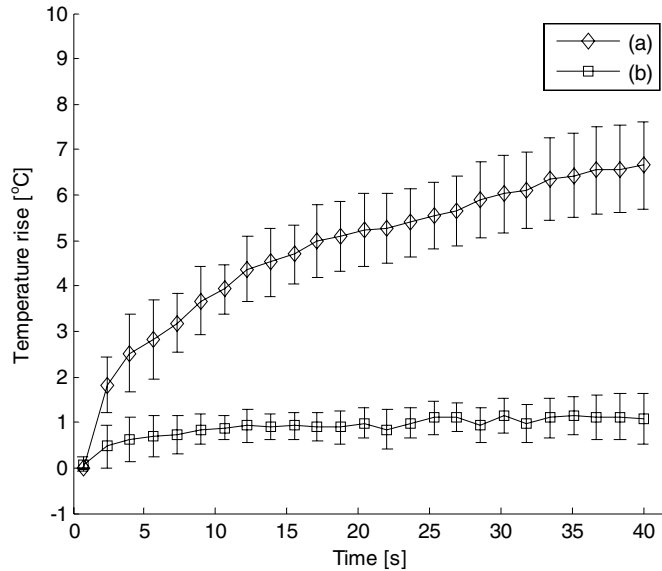


**Figure 6.** Comparison of temperature rise between two types of AM waves, a continuous AM wave (6(a)) and a pulsed AM wave (6(b)), both generated at the same low-acoustic intensity of  $231 \text{ W cm}^{-2}$ . The temperatures were measured at the focus of the FUS beam for a duration of 40 s. The application of a pulsed AM shows a relatively constant, low temperature ( $\Delta T \sim 1.2 \text{ }^\circ\text{C}$ ) compared to that induced by the continuous AM wave. Thus, a pulsed AM signal is suitable for tracking displacement before and after sonication.

beyond 10 s sonication, the lesion size is enough to display sufficient changes in the estimated displacement to clearly indicate irreversible tissue stiffening.

Figure 8 shows the equivalent M-mode image of the HMI displacement variation and pathology images after lesions were formed in *in vitro* liver specimens, using the therapy transducer to deliver a 10 s, 20 s or 30 s and exposure at  $1086 \text{ W cm}^{-2}$ . Figures 8(a), (c) and (e) show M-mode images obtained from the specimens throughout the entire treatment. The tissue depth is displayed along the vertical axis, and the observation time is displayed along the horizontal axis. HMI displacements sharply increase immediately after thermal treatment starts, then reach a peak and gradually decrease over time indicating lesion formation. Figure 9(a) portrays tissue displacements at the focal region for a 50 s continuous AM sonication. The pressure level of  $1086 \text{ W cm}^{-2}$  was used for the entire sonication and HMI was shown capable of following lesion formation during prolonged heating. Tissue softening occurred within the first 15 s (from 27 to 38 microns), followed by a rapid decrease in displacement indicating coagulation onset ( $\sim 18 \text{ } \mu\text{m}$ ) and tissue hardening beyond 30 s. The heating was stopped after 50 s and the liver was sectioned to verify tissue ablation (figure 9(b)).

Figure 10 is derived from the data shown in figure 8. The average HMI displacements at the focal region during thermal exposure are plotted as a function of temperature (lower axis) and thermal dose (upper axis). These graphs indicate that beyond  $45 \text{ }^\circ\text{C}$  the total displacement rose sharply by more than  $10 \text{ } \mu\text{m}$ . The slope (i.e., measured from the HMI displacement variation with temperature) during tissue softening (i.e., starting at the onset of heating), the plateau region and tissue hardening were  $3.5 \pm 0.12 \text{ } \mu\text{m } ^\circ\text{C}^{-1}$ ,  $0.4 \pm 0.27 \text{ } \mu\text{m } ^\circ\text{C}^{-1}$  and  $-0.53 \pm 0.056 \text{ } \mu\text{m } ^\circ\text{C}^{-1}$ , respectively. Figure 11(a) shows an example of the temperature and

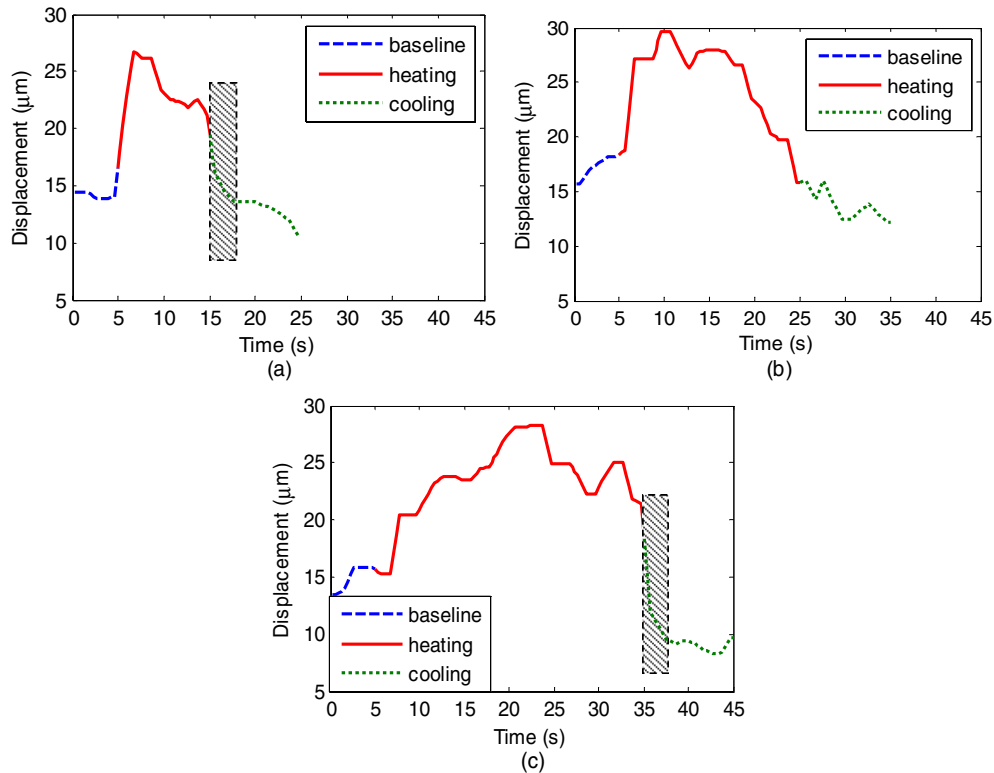


**Figure 7.** HMI displacement versus time. Blue (---), red (—) and green (···) lines indicate baseline (5 s), heating and cooling periods (10 s), respectively. Sonication duration varies from 10 s to 30 s (a to c) with an acquisition time step of 1 s.

HMI displacement profiles (figure 11(b)). A similar profile (for the displacement change from higher (figure 11, region I) to lower (figure 11, region II) values with increasing temperature) has been reported by Wu *et al* (2001). The arrow indicates the time sequence of the tissue displacement changes during heating and cooling.

## 5. Discussion

Thermal therapy using ultrasound techniques has been clinically applied for treatment of the prostate, liver and other cancers. In this paper, we demonstrated the potential of the HMIFU system for thermal ablation monitoring. The experimental results presented herein indicate the feasibility of using displacements induced by a radiation force for real-time monitoring of thermal lesion formation. The HMIFU system was applied with two distinct purposes. The first purpose was to obtain a baseline of the HMI displacement before and after thermal ablation. In this case, a low level of acoustic power (i.e., lower than the threshold of thermal ablation, equation (3)) was used to drive the therapy transducer, sufficient to induce adequate motion without significant heating (figure 6). In the second case, a higher power beam was applied to induce thermal ablation (figure 2). The main advantage of the HMIFU system was

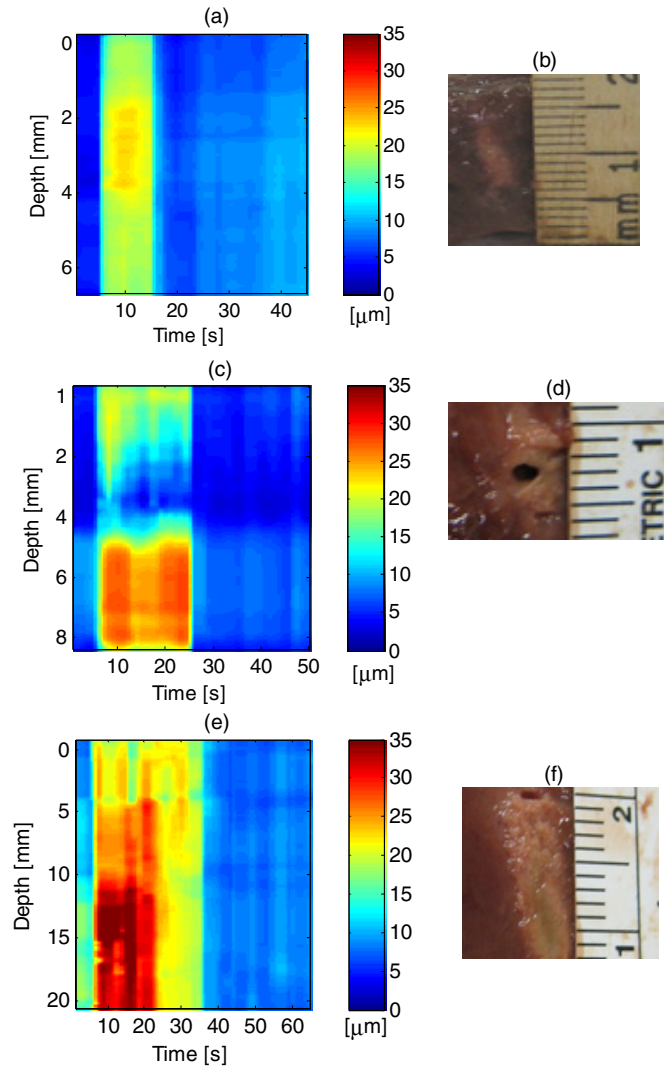


**Figure 8.** (a), (c) and (e) are the HMI displacement variation (M-mode) and (b), (d) and (f) are the corresponding pathology images of liver tissues for 10 s, 20 s and 30 s sonication, respectively.

that it could detect changes in tissue properties locally and with real-time feedback, while offering a flexible and more precise control of the thermal exposure.

The attenuation increase beyond coagulation (Damianou *et al* 1997) was ignored here. However, it did not interfere with the results reported since increased attenuation leads to greater radiation force, and thus displacement increase beyond coagulation; clearly, the opposite of what was observed with our method. Therefore, the stiffness change should override the attenuation change and thus, the attenuation change was assumed negligible (Konofagou *et al* 2003). In addition, Wu *et al* (2001) have shown that the tissue stiffness initially decreases with increasing temperature. When coagulative necrosis occurs, e.g., at a temperature beyond 50 °C, the tissue stiffness increases (Lizzi *et al* 2003, Fahey

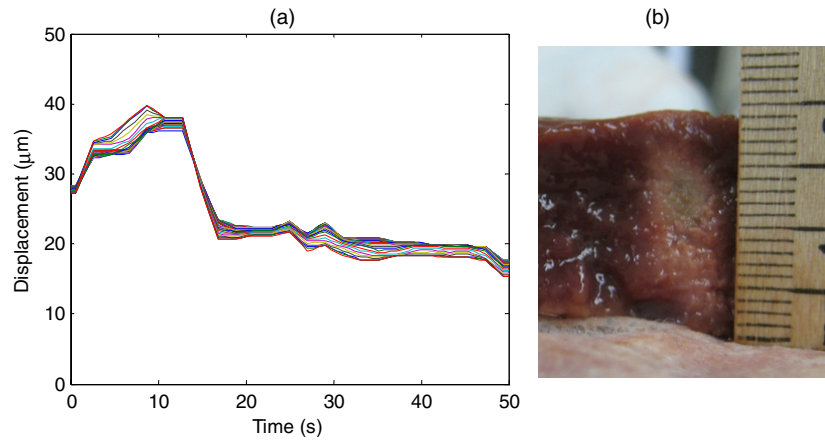


**Figure 9.** (a) HMI displacements at the focal region versus 50 s sonication time. (the 10 coloured lines indicate different locations (increments of 0.5 mm) at the focal region) (b) Pathology image of liver tissue after ablation.

**Table 1.** Summary of the slope (i.e., HMI displacement with temperature) and lesion sizes for 10 s, 20 s and 30 s exposures from seven bovine liver *in vitro* specimens.

Sonication duration (s)	Slope in the beginning of heating ( $\mu\text{m } ^\circ\text{C}^{-1}$ )	Slope during lesion formation ( $\mu\text{m } ^\circ\text{C}^{-1}$ )	Lesion size	
			Diameter (mm)	Length (mm)
10	$0.87 \pm 0.082$	$-0.88 \pm 0.080$	$2.0 \pm 0.12$	$6.4 \pm 1.14$
20	$0.85 \pm 0.12$	$-0.71 \pm 0.16$	$3.4 \pm 0.13$	$13.1 \pm 1.15$
30	$0.80 \pm 0.14$	$-0.79 \pm 0.19$	$4.7 \pm 0.18$	$16.4 \pm 0.39$

*et al* 2006). Our experimental results have shown a similar pattern on the displacement (or, relative tissue stiffness) variation with temperature during heating. In tissues, heat-absorption changes typically occur beyond  $50^\circ\text{C}$  ( $t_{43} = 2$  min; equation (3) (Damianou *et al* 1997). In the near field, where temperature elevation may occur at a slower rate during exposure, the change in absorption can be higher and the attenuation can change drastically (Damianou *et al* 1997).

At the beginning of thermal ablation, high temperature elevation caused a rapid increase in the HMI displacement (slope =  $0.8 \mu\text{m } ^\circ\text{C}^{-1}$ ), reached a peak and sometimes a plateau (depending on the duration of sonication), followed by a gradual decrease (slope =  $-0.79 \mu\text{m } ^\circ\text{C}^{-1}$ ), indicating coagulation. This slope reversal can be used to indicate the onset of lesion formation. Note that the slope of the displacement variation with temperature in the initial heating phase ( $0.8 \pm 0.11 \mu\text{m } ^\circ\text{C}^{-1}$ ) is reversed upon and during lesion formation ( $-0.79 \pm 0.14 \mu\text{m } ^\circ\text{C}^{-1}$ ) as shown in table 1; this effect can be used as an indication that the tissue mechanical properties have changed during sustained heating. The peak and the reversal of the slope could be detected by HMI during thermal ablation. This is important, especially since each region or type of tissue/organ has distinct thermal properties and thus, the changes in the slope might occur at different temperatures and sonication times.

Tissue displacements should increase during heating, reach a plateau, and decrease due to tissue necrosis (stiffening). However, in figures 7(a), (c), there were transient tissue displacements changing in the interval between after heating and the presence of necrosis

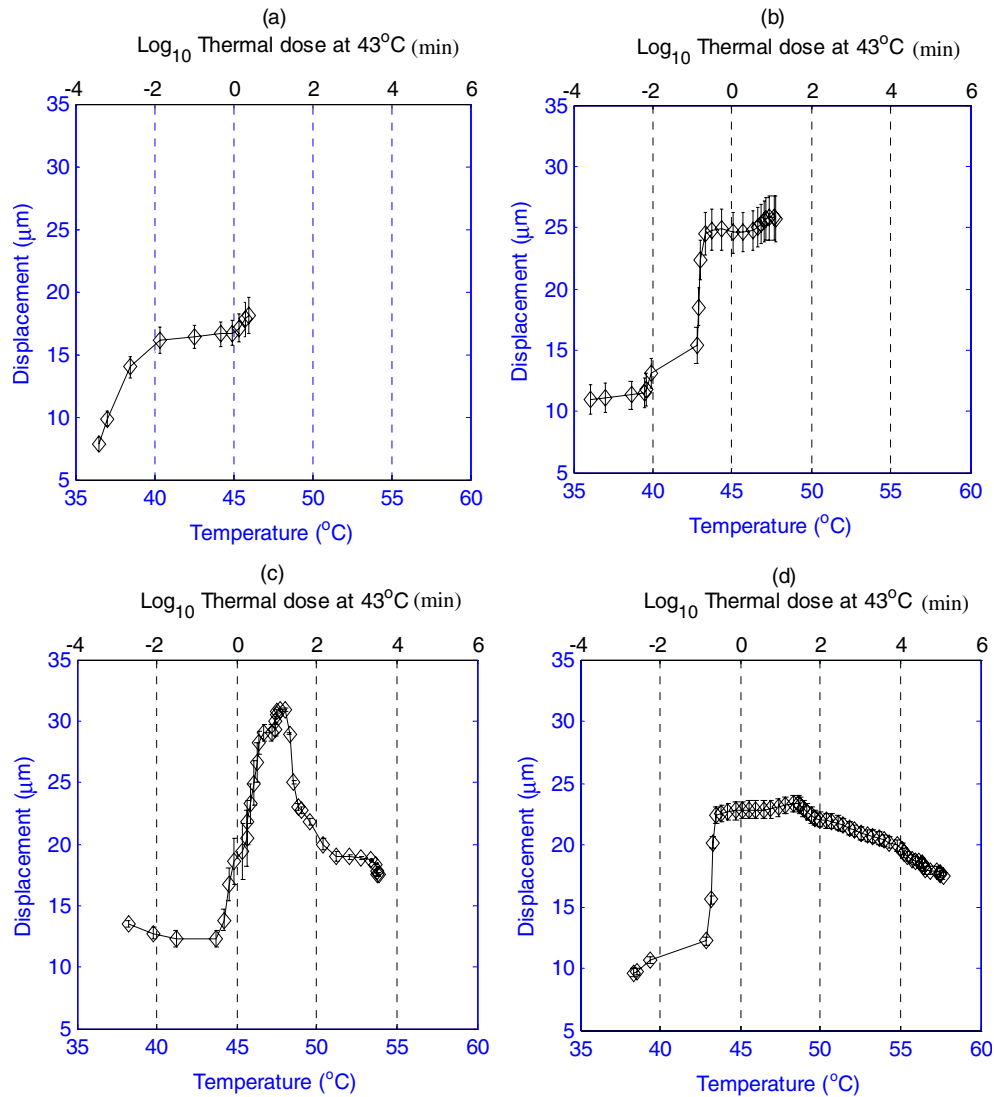


**Figure 10.** The relationship between temperature (or thermal dose ( $t_{43}$ ) in min) versus displacements for (a) 5 s, (b) 10 s, (c) 20 s and (d) 30 s sonication. Tissues started to soften at the initial heating (less than  $45^{\circ}\text{C}$ ) (a)–(d) and became stiffer (lesion (b)–(d)) at the temperatures above  $45^{\circ}\text{C}$  or  $t_{43} = 1$  min. The error bars are equal to one standard deviation.

(indicated by the gray region). When heating was terminated, the temperature rapidly decreased from  $50^{\circ}\text{C}$ , during which time the tissue was still coagulating, and therefore displacements further decreased from 18 to  $8\ \mu\text{m}$ . This technique is able to show that the lesion formation process is dependent on the tissue heterogeneity, which is one of the important conclusions of this study with respect to the HIFU treatment and the importance of its monitoring.

Figures 8(b), (c) show the absolute difference in displacements before and after ablation. However, figure 8(a) displays a relatively small lesion and tissue displacements slightly increase after 25 s of the cooling period. Tissue absorption changes after tissue coagulates

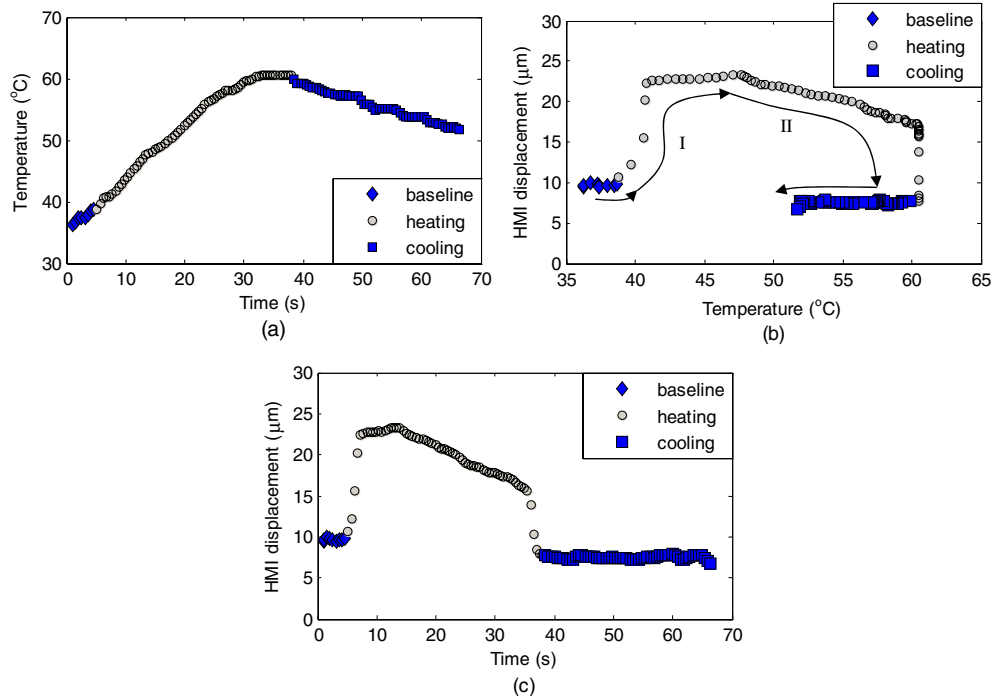


**Figure 11.** (a) Temperature versus time during 5 s (◆), 40 s heating (○) and 30 s cooling (■). (b) HMI displacement versus temperatures and (c) versus time in bovine liver *in vitro*.

(Bailey *et al* 2003). While the same low-intensity amplitude was used before and after heating, this absorption increase caused thus an increase in displacement while stiffening of the tissue (tissue necrosis presence) led to a decrease in displacement, i.e., the opposite effect from absorption. This trend is also shown in figure 9(a) when prolonged heating was used to sonicate liver tissue for 50 s. Since the size of the lesion formed is relatively small after 10 s sonication, the absorption effect becomes more dominant relative to the stiffness effect. Thus, the effects of absorption and stiffness are opposite and their combined effects on the HMI amplitude depend on the lesion size, as shown in our previously reported finite-element model (FEM) study (Maleke *et al* 2007). We thus consider this as a sensitivity limitation for our HMI technique, such that we are able to follow the changes in tissue stiffness after heating provided that the size of the necrosis is sufficiently large.

An interesting finding in the imaging and real-time capability of the proposed technique lie in the M-mode HMI analysis that can be used as a simple detection method to roughly map the spatio-temporal motion characteristics of the desired lesion (figure 8). This indicates that M-mode HMI images may be used as a real-time monitoring tool to visualize lesion formation during thermal ablation in real time. The M-mode images thus indicated the capability of detecting small changes in the tissue elastic properties and potentially mapping the stiffness change. Our experimental results demonstrated that after filtering the occurrence of the cavitation did not interfere with any of the data from the 21 locations in the bovine livers *in vitro*. Inertial or stable cavitation might occur at the subharmonic and/or higher harmonic frequencies. These subharmonics and harmonics may have thus been removed using the analog bandpass filter during acquisition. Thus, it was concluded that motion

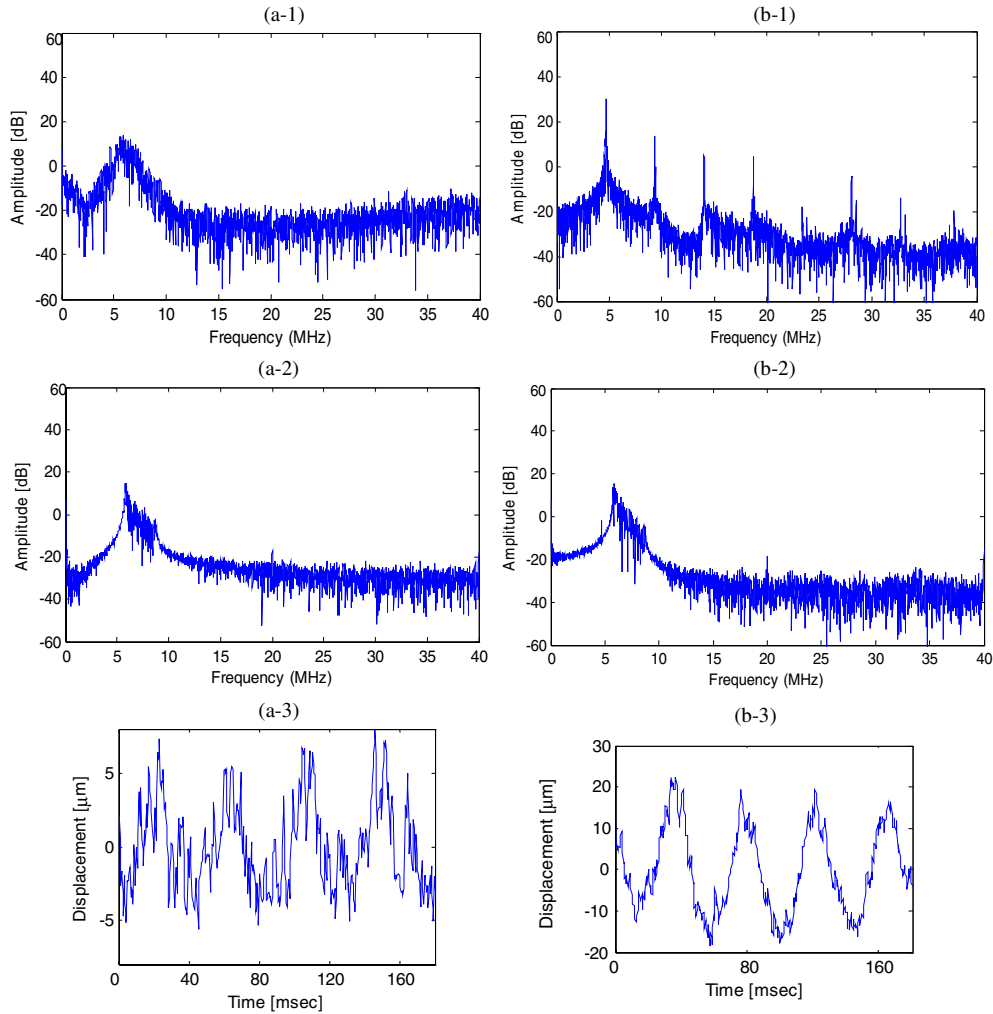


**Figure 12.** Before heating RF: spectra before (a-1) and (a-2) after bandpass filtering, (a-3) HMI displacement. During heating RF: spectra before (b-1) and (b-2) after bandpass filtering, (b-3) HMI displacement.

can be detected even in the potential presence of cavitation due to the type of filtering and modulation used.

Despite this, some precautions, such as the use of lower acoustic intensities and monitoring of temperature below  $65\text{ }^{\circ}\text{C}$ , were taken. The acoustic intensity that we used ( $251\text{--}1086\text{ W cm}^{-2}$ ) was lower compared to conventional HIFU powers currently being used ( $>1200\text{ W cm}^{-2}$ ) (Rabkin *et al* 2005). In all experiments performed, the HMI measurements were not significantly affected by cavitation effects during treatment, i.e., the displacements were estimated at high SNR throughout the entire treatment. There are two explanations for this. First, we use AM waves during both HMI and ablation procedures. This leads to lower power and smoother energy deposit, thus potentially reducing the probability of inertial cavitation. Second, the cavitation spectra are effectively removed when the pulse-echo spectrum (centered at  $7.5\text{ MHz}$ ) is filtered from the therapeutic one (centered at  $4.68\text{ MHz}$ )

using a bandpass analog filter (Reactel, Inc., Gaithersburg, Maryland, USA) with cutoff frequencies at  $f_{c1} = 5.84$  MHz and  $f_{c2} = 8.66$  MHz. The first assumption was verified through comparison of the lesion sizes between modulated and non-modulated configurations, with the former leading to smaller lesions. Two cases are shown in figure 12 to address the second assumption. The first case shows the RF spectrum and displacement before the HIFU treatment starts (figure 12(a)(1–3)). The second case shows the RF spectrum during the HIFU treatment (figure 12(b)(1–3)). Note that the displacement is reliably estimated both at the presence and absence of cavitation. A more thorough cavitation study verifying the robustness of the HMI method and the effect of bandpass filtering in the presence of cavitation is currently ongoing. The Matlab 7.0 (Mathworks inc., Natick, MA, USA) processing time needed in order to generate the M-mode displacement maps was approximately 30 s. Since the proposed technique is able to follow tissue stiffness changes during ablation, it would be advantageous to monitor the change in real time. Some improvements, such as a faster signal processing and the incorporation of a 1D linear array transducer for better target visualization during therapy, will be implemented in the future.

Important tissue parameters, such as the attenuation coefficient, which directly affect the force amplitude, and thus influence the induced tissue displacement, have not been included in this data analysis. Nevertheless, the experimental results presented here consistently showed that HMI could follow the thermal ablation process and detect the onset of lesion formation during the application of the thermal treatment. The aim of this technique is thus to monitor ablation non-invasively and efficiently with a real-time feedback during ablation. However, the technique is not limited to ultrasound therapy and can be applied with other thermal treatments, such as RF ablation or cryotherapy. Hyperechoic region from the RF catheter tip could be used as a treatment guidance reference to localize the treatment region. Further studies will involve finite-element simulations that will include all relevant parameters and *in vivo* application of HMIFU.

## 6. Conclusion

The HMIFU system has a simple transducer design that produces a constant oscillatory force at a focus within tissue using HMI for planning and monitoring of a thermal treatment. This technique has the ability of real-time synchronous monitoring of temperature-induced variation in tissue mechanical properties in a fully integrated system. By monitoring the HMI response in real time, the relative tissue stiffness changes during thermal treatment can be reliably indicated. The slope (displacement versus temperature) during the initial heating phase is reversed upon and during lesion formation. This effect can be used as an indication that the tissue mechanical properties have changed during sustained heating. M-mode HMI images may be an efficient and useful tool for visualizing lesion formation during thermal ablation. The ultimate future goal of this technique is simultaneous tumor localization as well as real-time monitoring of its ablation based on the associated tissue stiffness changes *in vivo*.

## Acknowledgments

This study was supported by a Special Development Award from the Whitaker Foundation and startup fund from Columbia University. The authors also wish to thank the Riverside Research Institute (RRI) for providing the transducers used for this study, and Dr Jianwen Luo for valuable discussions.

## References

- Anand A, Savery D and Hall C 2007 Three-dimensional spatial and temporal temperature imaging in gel phantoms using backscattered ultrasound *IEEE Trans. Ultrason. Ferroelectr. Freq. Control* **54** 23–31
- Arthur R M, Straube W L, Trobaugh J W and Moros E G 2005 Non-invasive estimation of hyperthermia temperatures with ultrasound *Int. J. Hyperth.* **21** 589–600
- Bailey M R, Khokhlova V A, Sapozhnikov O A, Kargl S G and Crum L A 2003 Physical mechanisms of the therapeutic effect of ultrasound—(a review) *Acoust. Phys.* **49** 369–88
- Bamber J C and Hill C R 1979 Ultrasonic attenuation and propagation speed in mammalian tissues as a function of temperature *Ultrasound Med. Biol.* **5** 149–57
- Bercoff J, Pernot M, Tanter M and Fink M 2004a Monitoring thermally-induced lesions with supersonic shear imaging *Ultrason. Imaging* **26** 71–84
- Bercoff J, Tanter M and Fink M 2004b Supersonic shear imaging: a new technique for soft tissue elasticity mapping *IEEE Trans. Ultrason. Ferroelectr. Freq. Control* **51** 396–409
- Burov A K and Andreevskaya G D 1956 Effect of high intensity supersonic oscillations on malignant tumors in man and animals *Dokl. Akad. Nauk SSSR* **106** 445–8
- Chapelon J Y, Margonari J, Vernier F, Gorry F, Ecochard R and Gelet A 1992 *In vivo* effects of high-intensity ultrasound on prostatic adenocarcinoma dunning R3327 *Cancer Res.* **52** 6353–7
- Chavrier F, Chapelon J Y, Gelet A and Cathignol D 2000 Modeling of high-intensity focused ultrasound-induced lesions in the presence of cavitation bubbles *J. Acous. Soc. Am.* **108** 432–40
- Christensen DA 1988 *Ultrasonic Bioinstrumentation* (New Jersey: Wiley)
- Cline H E, Hynynen K, Watkins R D, Adams W J, Schenck J F, Ettinger R H, Freund W R, Vetro J P and Jolesz F A 1995 Focused US system for MR imaging-guided tumor ablation *Radiology* **194** 731–7
- Corry P M, Jabboury K, Armour E P and Kong J S 1984 Human cancer-treatment with ultrasound *IEEE Trans. Ultrason. Ferroelectr. Freq. Control* **31** 444–56
- Damianou C A, Sanghvi N T, Fry F J and MaassMoreno R 1997 Dependence of ultrasonic attenuation and absorption in dog soft tissues on temperature and thermal dose *J. Acoust. Soc. Am.* **102** 628–34
- Fahey B J, Hsu S J, Wolf P D, Nelson R C and Trahey G E 2006 Liver ablation guidance with acoustic radiation force impulse imaging: challenges and opportunities *Phys. Med. Biol.* **51** 3785–808
- Fahey B J, Nightingale K R, Stutz D L and Trahey G E 2004 Acoustic radiation force impulse imaging of thermally- and chemically-induced lesions in soft tissues: preliminary *ex vivo* results *Ultrasound Med. Biol.* **30** 321–8
- Fatemi M and Greenleaf J F 1998 Ultrasound-stimulated vibro-acoustic spectrography *Science* **280** 82–85
- Fatemi M and Greenleaf J F 2000 Probing the dynamics of tissue at low frequencies with the radiation force of ultrasound *Phys. Med. Biol.* **45** 1449–64
- Frizzell L A 1988 Threshold dosages for damage to mammalian liver by high-intensity focused ultrasound *IEEE Trans. Ultrason. Ferroelectr. Freq. Control* **35** 578–81
- Fry W J, Barnard J W, Fry F J, Krumin R F and Brennan J F 1955 Ultrasonic lesions in the mammalian central nervous system *Science* **122** 517–8
- Fry F J and Johnson L K 1978 Tumor irradiation with intense ultrasound *Ultrasound Med. Biol.* **4** 337–41
- Fry W J, Mosberg W H, Barnard J W and Fry F J 1954 Production of focal destructive lesions in the central nervous system with ultrasound *J. Neurosurg.* **11** 471–8
- Furusawa H, Namba K, Thomsen S, Akiyama F, Bendet A, Tanaka C, Yasuda Y and Nakahara H 2006 Magnetic resonance-guided focused ultrasound surgery of breast cancer: reliability and effectiveness *J. Am. Coll. Surg.* **203** 54–63
- Gelet A, Chapelon J Y, Bouvier R, Pangaud C and Lasne Y 1999 Local control of prostate cancer by transrectal high intensity focused ultrasound therapy: preliminary results *J. Urol.* **161** 156–62
- Gelet A, Chapelon J Y, Bouvier R, Souchon R, Pangaud C, Abdelrahim A F, Cathignol D and Dubernard J M 1996 Treatment of prostate cancer with transrectal focused ultrasound: early clinical experience *Eur. Urol.* **29** 174–83
- Gellermann J, Wlodarczyk W, Feussner A, Fahling H, Nadobny J, Hildebrandt B, Felix R and Wust P 2005 Methods and potentials of magnetic resonance imaging for monitoring radiofrequency hyperthermia in a hybrid system *Int. J. Hypertherm.* **21** 497–513
- Gianfelice D, Khiat A, Amara M, Belblidia A and Boulanger Y 2003 MR imaging-guided focused ultrasound surgery of breast cancer: correlation of dynamic contrast-enhanced MRI with histopathologic findings *Breast Cancer Res. Treat.* **82** 93–101
- Goss S A and Fry F J 1984 The Effect of High-Intensity Ultrasonic Irradiation on Tumor-Growth *IEEE Trans. Ultrason. Ferroelectr. Freq. Control* **31** 491–6
- Hall T J, Bilgen M, Insana M F and Krouskop T A 1997 Phantom materials for elastography *IEEE Trans. Ultrason. Ferroelectr. Freq. Control* **44** 1355–65

- Hill C R and Ter Haar G R 1995 Review article: high intensity focused ultrasound-potential for cancer treatment *Br. J. Radiol.* **68** 1296–303
- Huber P E, Jenne J W, Rastert R, Simiantonakis I, Sinn H P, Strittmatter H J, von Fournier D, Wannenmacher M F and Debus J 2001 A new noninvasive approach in breast cancer therapy using magnetic resonance imaging-guided focused ultrasound surgery *Cancer Res.* **61** 8441–7
- Hynynen K 1997 Review of ultrasound therapy *Ultrasonics Symp. 1997 IEEE (Ontario, Canada)* pp 1305–13
- Hynynen K, Pomeroy O, Smith D N, Huber P E, McDannold N J, Kettenbach J, Baum J, Singer S and Jolesz F A 2001 MR imaging-guided focused ultrasound surgery of fibroadenomas in the breast: A feasibility study *Radiology* **219** 176–85
- Kallel F, Stafford R J, Price R E, Righetti R, Ophir J and Hazle J D 1999 The feasibility of elastographic visualization of HIFU-induced thermal lesions in soft tissues *Ultrasound Med. Biol.* **25** 641–7
- Kennedy J E 2005 High-intensity focused ultrasound in the treatment of solid tumours *Nat. Rev. Cancer* **5** 321–327
- Kennedy J E, Ter Haar G R and Cranston D 2003 High intensity focused ultrasound: surgery of the future? *Br. J. Radiol.* **76** 590–9
- Konofagou E E and Hynynen K 2002 Localized harmonic motion imaging: theory, simulations and experiments *Ultrasonics Symp. 2002 IEEE (Munich, Germany)* pp 1895–8
- Konofagou E E and Hynynen K 2003 Localized harmonic motion imaging: theory, simulations and experiments *Ultrasound Med. Biol.* **29** 1405–1413
- Konofagou E E, Thierman J and Hynynen K 2001 A focused ultrasound method for simultaneous diagnostic and therapeutic applications—a simulation study *Phys. Med. Biol.* **46** 2967–84
- Konofagou E E, Thierman J and Hynynen K 2003 The use of ultrasound-stimulated acoustic emission in the monitoring of modulus changes with temperature *Ultrasonics* **41** 337–45
- Konofagou E E, Thierman J, Karjalainen T and Hynynen K 2002 The temperature dependence of ultrasound-stimulated acoustic emission *Ultrasound Med. Biol.* **28** 331–8
- Krouskop T A, Wheeler T M, Kallel F, Garra B S and Timothy H 1998 Elastic moduli of breast and prostate tissues under compression *Ultrason. Imaging* **20** 260–74
- Lele P P 1966 Concurrent detection of the production of ultrasonic lesions *Med. Biol. Eng.* **4** 451–6
- Lele P P 1967 Production of deep focal lesions by focused ultrasound-current status *Ultrasonics* **5** 105–10
- Lewa C J 1991 Magnetic-resonance-imaging in the presence of mechanical waves *Spectrosc. Lett.* **24** 55–67
- Linke C A, Carstens E L, Frizzell L A, Elbadawi A and Fridd C W 1973 Localized tissue destruction by high-intensity focused ultrasound *Arch. Surg.* **107** 887–891
- Lizzi F L, Muratore R, Deng C X, Ketterling J A, Alam S K, Mikaelian S and Kalisz A 2003 Radiation-force technique to monitor lesions during ultrasonic therapy *Ultrasound Med. Biol.* **29** 1593–605
- Lynn J G and Putnam T J 1944 Histology of cerebral lesions produced by focused ultrasound *Am. J. Pathol.* **20** 637–49
- Lynn J G, Zwemer R L, Chick A J and Miller A E 1943 A new method for the generation and use of focused ultrasound in experimental biology *J. Gen. Physiol.* **26** 179–93
- Madersbacher S, Pedevilla M, Vingers L, Susani M and Mrberger M 1995 Effect of high-intensity focused ultrasound on human prostate-cancer *in vivo* *Cancer Res.* **55** 3346–51
- Maleke C, Luo J, Pelegri M and Konofagou E 2007 Mapping of regional tissue mechanical changes using harmonic motion imaging *ASME Int. Mechanical Engineering Congress and Exposition (Seattle, WA)*
- Maleke C, Pernot M and Konofagou E E 2006 Single-element focused ultrasound transducer method for harmonic motion imaging *Ultrason. Imaging* **28** 144–58
- Michishita K, Hasegawa H and Kanai H 2003 Ultrasonic measurement of minute displacement of object cyclically actuated by acoustic radiation force *Japan J. Appl. Phys. Part I* **42** 4608–12
- Muthupillai R, Lomas D J, Rossman P J, Greenleaf J F, Manduca A and Ehman R L 1995 Magnetic-resonance elastography by direct visualization of propagating acoustic strain waves *Science* **269** 1854–7
- Nightingale K R, Palmeri M L, Nightingale R W and Trahey G E 2001 On the feasibility of remote palpation using acoustic radiation force *J. Acoust. Soc. Am.* **110** 625–34
- Ophir J, Céspedes I, Ponnekanti H, Yazdi Y and Li X 1997 Elastography: a method for imaging the elasticity of biological tissues *Ultrason. Imaging* **13** 111–34
- Pernot M, Tanter M, Bercoff J, Waters K R and Fink M 2004 Temperature estimation using ultrasonic spatial compound imaging *IEEE Trans. Ultrason. Ferroelectr. Freq. Control* **51** 606–15
- Rabkin B A, Zderic V and Vaezy S 2005 Hyperecho in ultrasound images of HIFU therapy: involvement of cavitation *Ultrasound Med. Biol.* **31** 947–56
- Righetti R, Kallel F, Stafford R J, Price R E, Krouskop T A, Hazle J D and Ophir J 1999 Elastographic characterization of HIFU-induced lesions in canine livers *Ultrasound Med. Biol.* **25** 1099–113
- Rivens I, Shaw A, Civale J and Morris H 2007 Treatment monitoring and thermometry for therapeutic focused ultrasound *Int. J. Hyperth.* **23** 121–39

- Sanghvi N T, Fry F J, Bihrlé R, Foster R S, Phillips M H, Syrus J, Zaitsev A V and Hennige C W 1996 Noninvasive surgery of prostate tissue by high-intensity focused ultrasound *IEEE Trans. Ultrason. Ferroelectr. Freq. Control* **43** 1099–110
- Sapareto S A and Dewey W C 1984 Thermal Dose Determination in Cancer-Therapy *Int. J. Radiat. Oncol. Biol. Phys.* **10** 787–800
- Sarvazyan A P, Rudenko O V, Swanson S D, Fowlkes J B and Emelianov S Y 1998 Shear wave elasticity imaging: a new ultrasonic technology of medical diagnostics *Ultrasound Med. Biol.* **24** 1419–35
- Seip R and Ebbini E S 1995 Noninvasive estimation of tissue temperature response to heating fields using diagnostic ultrasound *IEEE Trans. Biomed. Eng.* **42** 828–39
- Seip R, VanBaren P, Cain C A and Ebbini E 1996 Noninvasive real-time multipoint temperature control for ultrasound phased array treatments *IEEE Trans. Ultrason. Ferroelectr. Freq. Control* **43** 1063–73
- Sinkus R, Bercoff J, Tanter M, Gennisson J L, El Khoury C, Servois V, Tardivon A and Fink M 2006 Nonlinear viscoelastic properties of tissue assessed by ultrasound *IEEE Trans. Ultrason. Ferroelectr. Freq. Control* **53** 2009–18
- Sinkus R, Lorenzen J, Schrader D, Lorenzen M, Dargatz M and Holz D 2000 High-resolution tensor MR elastography for breast tumour detection *Phys. Med. Biol.* **45** 1649–64
- Souchon R, Rouviere O, Gelet A, Detti V, Srinivasan S, Ophir J and Chapelon J Y 2003 Visualisation of hifu lesions using elastography of the human prostate *in vivo*: preliminary results *Ultrasound Med. Biol.* **29** 1007–15
- Stafford R J, Kallel F, Price R E, Cromeens D M, Krouskop T A, Hazle J D and Ophir J 1998 Elastographic imaging of thermal lesions in soft tissue: a preliminary study *in vitro* *Ultrasound Med. Biol.* **24** 1449–58
- Taylor K J W and Connolly C C 1969 Differing hepatic lesions caused by same dose of ultrasound *J. Pathol.* **98** 291–3
- Ter Haar G 1995 Ultrasound focal beam surgery *Ultrasound Med. Biol.* **21** 1089–100
- Ter Haar G, Sinnott D and Rivens I 1989 High-intensity focused ultrasound—a surgical technique for the treatment of discrete liver-tumors *Phys. Med. Biol.* **34** 1743–50
- Vaezy S *et al* 1997 Liver hemostasis using high-intensity focused ultrasound *Ultrasound Med. Biol.* **23** 1413–20
- Vykhodtseva N I, Hynynen K and Damianou C 1995 Histologic effects of high-intensity pulsed ultrasound exposure with subharmonic emission in rabbit brain *in-vivo* *Ultrasound Med. Biol.* **21** 969–79
- Wu F 2006 Extracorporeal high intensity focused ultrasound in the treatment of patients with solid malignancy *Min. Invasive Therm. Allied Technol.* **15** 26–35
- Wu T, Felmlee J P, Greenleaf J F, Riederer S J and Ehman R L 2001 Assessment of thermal tissue ablation with MR elastography *Magn. Reson. Med.* **45** 80–7
- Yang R, Kopecky K K, Rescorla F J, Galliani C A, Wu E X and Grosfeld J L 1993 Sonographic and computed-tomography characteristics of liver ablation lesions induced by high-intensity focused ultrasound *Invest. Radiol.* **28** 796–801